

See discussions, stats, and author profiles for this publication at: <https://www.researchgate.net/publication/350372805>

Green Synthesis of Zinc Oxide (ZnO) Nanoparticles Using Aqueous Fruit Extracts of *Myristica fragrans*: Their Characterizations and Biological and Environmental Applications

Article in ACS Omega · March 2021

CITATION

1

READS

188

12 authors, including:



Hasnain Jan

National Taiwan University

34 PUBLICATIONS 311 CITATIONS

[SEE PROFILE](#)



Sumaira Shah

34 PUBLICATIONS 207 CITATIONS

[SEE PROFILE](#)



Muhammad Taj Akbar

Abdul Wali Khan University Mardan

23 PUBLICATIONS 82 CITATIONS

[SEE PROFILE](#)



Muhammad Rizwan

University of Swat

74 PUBLICATIONS 455 CITATIONS

[SEE PROFILE](#)

Some of the authors of this publication are also working on these related projects:



[Nano-medicines and Nano-toxicology](#) [View project](#)



[Rheumatoid Arthritis](#) [View project](#)

1 Green Synthesis of Zinc Oxide (ZnO) Nanoparticles Using Aqueous 2 Fruit Extracts of *Myristica fragrans*: Their Characterizations and 3 Biological and Environmental Applications

4 Shah Faisal,* Hasnain Jan, Sajjad Ali Shah, Sumaira Shah, Adan Khan, Muhammad Taj Akbar,
5 Muhammad Rizwan, Faheem Jan, Wajid Ullah, Noreen Akhtar, Aishma Khattak, and Suliman Syed



Cite This: <https://doi.org/10.1021/acsomegaj.1c00310>



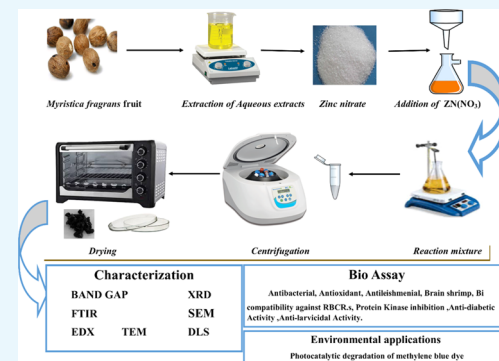
Read Online

ACCESS |

Metrics & More

Article Recommendations

6 **ABSTRACT:** In the present work, bioaugmented zinc oxide nanoparticles
7 (ZnO-NPs) were prepared from aqueous fruit extracts of *Myristica fragrans*. The
8 ZnO-NPs were characterized by different techniques such as X-ray diffraction
9 (XRD), Fourier transform infrared (FTIR) spectroscopy, ultraviolet (UV)
10 spectroscopy, scanning electron microscopy (SEM), transmission electron
11 microscopy (TEM), dynamic light scattering (DLS), and thermogravimetric
12 analysis (TGA). The crystallites exhibited a mean size of 41.23 nm measured via
13 XRD and were highly pure, while SEM and TEM analyses of synthesized NPs
14 confirmed their spherical or elliptical shape. The functional groups responsible for
15 stabilizing and capping of ZnO-NPs were confirmed using FTIR analysis. The ζ -
16 size and ζ -potential of synthesized ZnO-NPs were reported as 66 nm and -22.1
17 mV, respectively, via the DLS technique can be considered as moderate stable
18 colloidal solution. Synthesized NPs were used to evaluate for their possible
19 antibacterial, antidiabetic, antioxidant, antiparasitic, and larvicidal properties. The NPs were found to be highly active against
20 bacterial strains both coated with antibiotics and alone. *Klebsiella pneumoniae* was found to be the most sensitive strain against NPs
21 (27 ± 1.73) and against NPs coated with imipinem (26 ± 1.5). ZnO-NPs displayed outstanding inhibitory potential against enzymes
22 protein kinase (12.23 ± 0.42), α -amylase (73.23 ± 0.42), and α -glucosidase (65.21 ± 0.49). Overall, the synthesized NPs have
23 shown significant larvicidal activity (77.3 ± 1.8) against *Aedes aegypti*, the mosquitoes involved in the transmission of dengue fever.
24 Similarly, tremendous leishmanicidal activity was also observed against both the promastigote (71.50 ± 0.70) and amastigote (61.41
25 ± 0.71) forms of the parasite. The biosynthesized NPs were found to be excellent antioxidant and biocompatible nanomaterials.
26 Biosynthesized ZnO-NPs were also used as photocatalytic agents, resulting in 88% degradation of methylene blue dye in 140 min.
27 Owing to their eco-friendly synthesis, nontoxicity, and biocompatible nature, ZnO-NPs synthesized from *M. fragrans* can be
28 exploited as potential candidates for biomedical and environmental applications.



29 ■ INTRODUCTION

30 Nanotechnology is now considered to be a proven state-of-the-
31 art technology with numerous branches embedded in
32 industrial fields such as chemical, pharmaceutical, mechanical,
33 and food processing industries. Nanotechnology also plays an
34 interesting role in the areas of computing, power generation,
35 optics, drug delivery, and environmental sciences.¹ In the
36 advent of nanotechnology, many nanoscale devices have been
37 developed using numerous methods, such as physical,
38 chemical, and green approaches. Yet, green nanoparticle
39 synthesis is a tool of choice that can be easily prepared and
40 engineered.² There are many drawbacks of conventional
41 approaches for the synthesis of nanoparticles, including long-
42 term processing, high cost, laborious procedures, and in
43 particular the use of toxic compounds. Most of the relevant
44 study has been directed to eco-friendly and fast synthesis
45 protocols for the production of nanoparticles due to these

46 limitations.^{3,4} For material scientists, the development of eco-
friendly methods for synthesizing nanoscale materials has been
47 a major focus in recent years. In this respect, green synthesis of
48 NPs, especially using extracts from different plants, is a
49 growing trend that is considered simple, cheap, and nontoxic in
50 green chemistry.^{5–7} Nanotechnology has also increased the
51 human standard of living by addressing many everyday life
52 issues, such as the contribution to energy sufficiency; climate
53

Received: January 18, 2021

Accepted: March 15, 2021

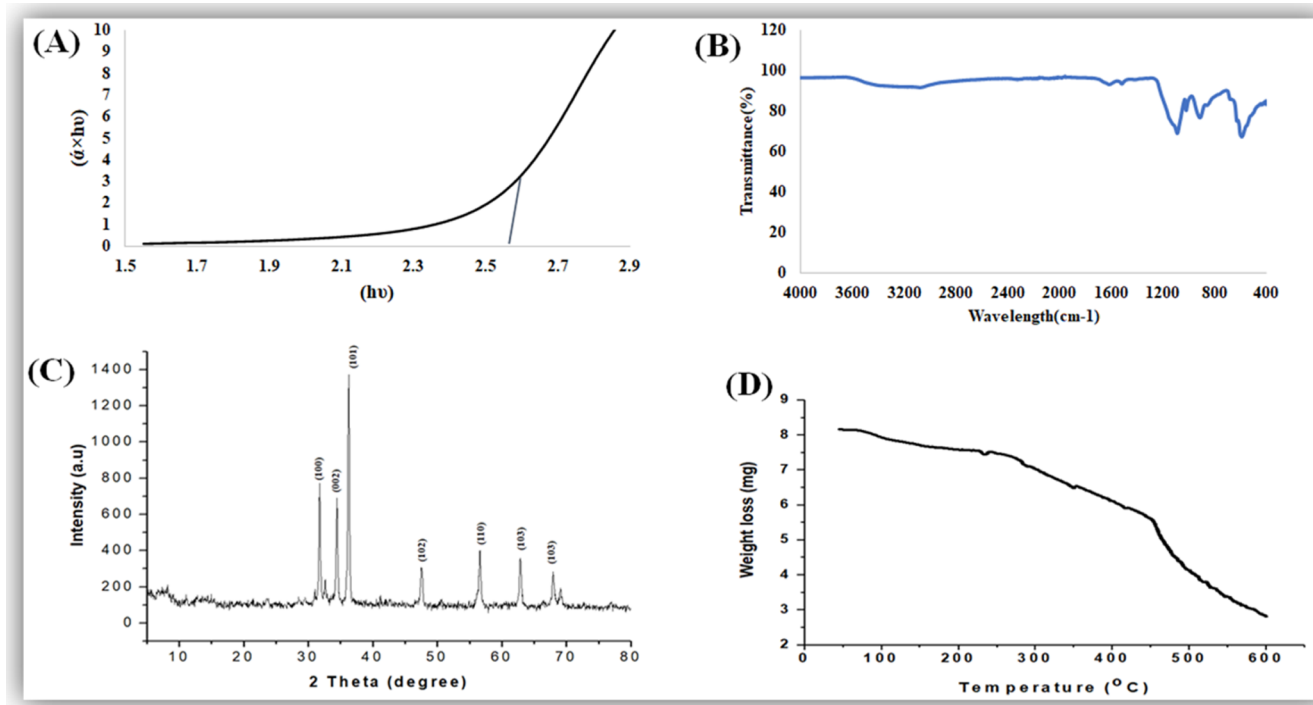


Figure 1. (A) UV band gap, (B) typical FTIR spectra, (C) typical XRD pattern, and (D) typical TGA pattern of *M. fragrans* fruit-synthesized ZnO-NPs.

54 change; beauty, textile, and health industries including the cure
 55 of deadly diseases such as cancers and Alzheimer's.^{8,9}

56 Due to their multiple applications in various technical fields,
 57 comprehensive investigation into metal oxide nanoparticles has
 58 been concentrated in the past decade.¹⁰ Among these, with
 59 multifaceted benefits, ZnO-NPs are exciting inorganic
 60 materials. ZnO-NPs can be used in various sectors, such as
 61 energy conservation, textiles, electronics, healthcare, catalysis,
 62 cosmetics, semiconductors, and chemical sensing.^{11–15} The
 63 NPs are nontoxic and biocompatible and display excellent
 64 biomedical applications, such as anticancer,¹⁶ anti-inflammatory,
 65 and antimicrobial properties, in targeted drug
 66 delivery,¹⁷ wound healing, and bioimaging.^{19,20}

67 Nanoproducts can be produced from different methods
 68 (chemical, physical, and biosynthesis) with multiple properties
 69 and huge applications. Plant-based synthesis of ZnO-NPs has
 70 previously been reported though, inadequate literature is
 71 existing on their diverse biological properties such as
 72 antimicrobial, antilarvicidal, protein kinase, and anticancer
 73 activities. The curative uses of *Myristica fragrans* (Jaiphal) are
 74 well known, and it is mainly used as an anti-inflammatory,
 75 antidiarrheal, analgesic, and sex stimulant agent.²¹

76 Here, we report plant-based synthesis of zinc oxide
 77 nanoparticles using the aqueous extracts of *M. fragrans* fruits.
 78 Green synthesis of ZnO-NPs has eco-friendly aspects and
 79 various biomedical applications. The metabolites found in the
 80 aqueous extract of *M. fragrans* act as an oxidizing, reducing,
 81 and capping agent for the synthesis of biogenic ZnO-NPs. The
 82 green synthesized nanoparticles will be characterized using
 83 modern techniques such as Fourier transform infrared (FTIR)
 84 spectroscopy, ultraviolet (UV) spectroscopy, X-ray diffraction
 85 (XRD), scanning electron microscopy (SEM), transmission
 86 electron microscopy (TEM), dynamic light scattering (DLS),
 87 and thermal gravimetric analysis (TGA). The NPs will be
 88 checked for their antimicrobial, antileishmanial, antidiabetic,

89 antioxidant, antilarvicidal, and protein kinase inhibitory
 90 potential.

RESULTS AND DISCUSSION

Biosynthesis of ZnO-NPs. *M. fragrans* is known as “nutmeg”; its extracts and essential oils are important in drug development with numerous pharmacological activities in South Africa, India, and other tropical countries.²² For a long time, *M. fragrans* has been used in traditional medicines as a carminative, stimulant, narcotic, emmenagogue, and abortifacient. Nutmeg is also prescribed for the treatment of many diseases, such as rheumatism, muscle spasm, decreased appetite, and diarrhea. *M. fragrans* has recently been shown to have antioxidant, anticonvulsant, analgesic, anti-inflammatory, antidiabetic, antibacterial, and antifungal activities. Trimyristin, myristic acid, myristicin, safrole, and elemicin are reported from nutmeg. Due to the easy collection of nutmeg, widespread presence, and also remarkable biological activities, it has become both food and medicine in tropical countries, especially in India and China.^{22,23} The biosynthesis of zinc oxide nanoparticles was carried out using aqueous fruit extracts of *M. fragrans* as reducing, capping, and stabilizing agents.²⁴ Broad studies disclose that volatile oils are the major constituents within the dry biomass of *M. fragrans*. Among numerous constituents, D-pinene, myristin, and myristic acid and its esters contribute to the high percentage of the dry weight. Moreover, myristicin, fatty acids, and mesin constitute one-half of the dry biomass.^{25–27} It is assumed that the constituents present in *M. fragrans* biomass have contributed a lot in the preparation of eco-friendly and biomedically important zinc oxide nanoparticles. When the reaction is carried out between Zn(NO₃)₂·2H₂O and *M. fragrans*, the color of the mixture changes from light brown to dark gray, which confirms the formation of zinc oxide nanoparticles.

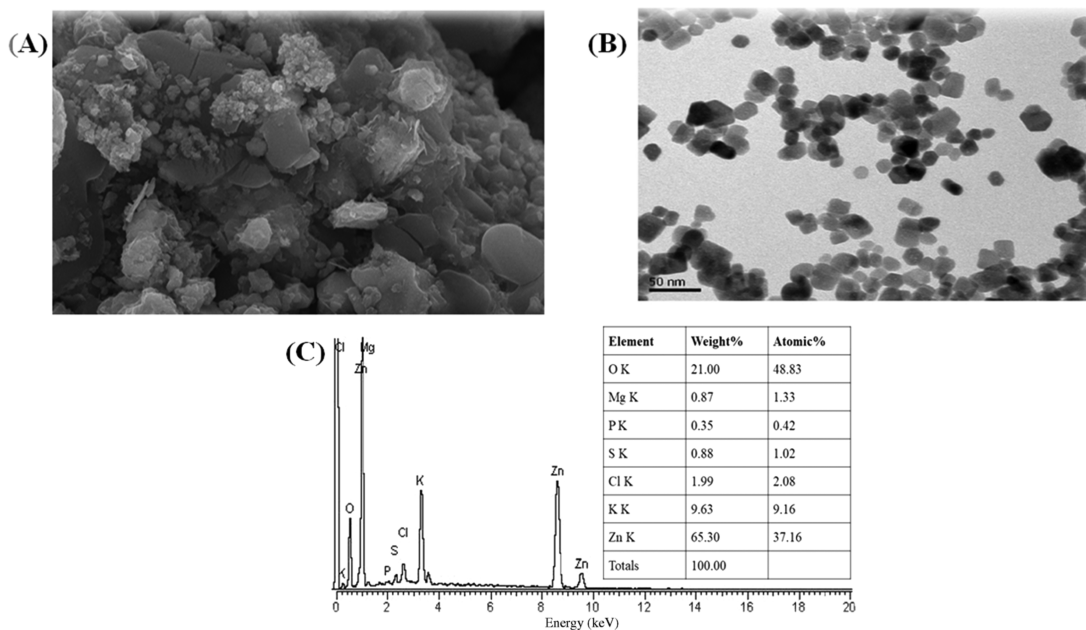


Figure 2. (A) SEM micrograph, (B) TEM micrograph, and (C) EDX spectrograph of *M. fragrans* fruit-synthesized ZnO-NPs.

(ZnO-NPs).²⁸ After subsequent steps of washing, drying, grinding, and calcination, white powder of ZnO-NPs was obtained. The fine powder collected was stored in an airtight glass vial, labeled as ZnO-NPs, at room temperature for physicochemical and morphological characterizations and biological applications. The literature study revealed that physicochemical and morphological characteristics of ZnO-NPs mainly depend on the type and species of plant used and the reaction conditions such as the pH, temperature, and synthesis medium.²⁹

Band Gap. The band gap of ZnO-NPs is characterized by performing UV-visible spectroscopy. The particles show a very sharp band gap, which was 2.57 eV. The smaller band gap will easily categorize a photocatalytic reaction of the nano-particles and show good photocatalytic activity for the degradation of methylene blue dye, as shown in Figure 1A. Because of the smaller band gap, the electron is easily excited from the valence band to the conduction band. In the previous literature, it was reported in ref 30 by performing UV spectroscopy on ZnO-NPs that the band gap obtained was 3.29 eV. The Tauc plot method was used to calculate the band gap, as shown in Figure 1A, which is very close to the value reported in the literature.^{31,32} The band gap depends on various factors, including the grain size, oxygen deficiency, surface roughness, and lattice strain.³³

Fourier Transform Infrared (FTIR) Spectroscopy. To classify functional groups in the aqueous extract and zinc oxide nanoparticles, we perform FTIR spectroscopy in the range of 4000–400 cm^{-1} , as shown in Figure 1B. The peak of ZnO obtained at 469 cm^{-1} could be due to zinc and oxygen bonding vibrations.³⁴ The low absorption peak observed at around 3420 and 3200 cm^{-1} could be appointed to hydroxyl (OH) groups; also, some other bands were observed at around 1600, 1100, and 900 cm^{-1} . A major change in IR spectra was noticed in this range. A deep absorbance band at 1100 indicates the presence of carbohydrate (C–O), (C=C) rings (polysaccharides, pectin, and cellulose). Both primary and secondary metabolites are present in the plant body abundantly. A peak at 900 encompasses the phosphodiester stretching band region

(for absorbance due to collagen and glycogen).³⁵ The phosphodiester bond is a linkage between 3' C and 5' C atoms in deoxyribose and ribose sugar in DNA and RNA, respectively. The polysaccharide carbohydrates (glycogen) have strong binding ability with metal (Zn) and create a layer on its surface to prevent its agglomeration in the reaction medium.³⁶

X-ray Diffraction (XRD) Analysis. The X-ray diffraction pattern of zinc oxide nanoparticles shows definite line broadening of the X-ray diffraction peaks, showing that the prepared particles were in the nanoscale range, as shown in Figure 1C. The diffraction peaks located at 31.5, 34.4, 36.2, 47.5, 56.4, 62.8, and 67.9° have been indexed as the spherical to the hexagonal phase of ZnO with high crystallinity^{37,38} with (JPCDS card number 36-1451). It was revealed that all of the characteristic peaks were of ZnO-NPs, and no such impurities exist in synthesized ZnO-NPs. The diameter of zinc oxide crystallites was calculated by the Debye–Scherrer formula. On the bases of θ (Bragg's diffraction angle) and β (full width at half-maximum (FWHM)) of more intense peaks corresponding to 101 planes located at position 36.2°, the crystallite size is about 29 nm,³⁹ while the average crystallite size is 41.23 nm. The indexation confirms the standard hexagonal wurtzite structure (JCPDF file no. 00-036-1451) of ZnO-NPs, as previously reported in other studies.⁴⁰

Thermogravimetric Analysis (TGA). The TGA spectra of ZnO-NPs indicate that the sample decomposes greatly with an increase in temperature. The sample (5 mg) was totally decomposed up to 600 °C loss; it was due to the different volatile components present in the sample from the plant, as shown in Figure 1D. The initial loss of the sample was due to the presence of ethanol and water in the sample. Similar weight loss was also reported by ref 41, who synthesized ZnO-NPs using aqueous extracts of *Mimosa pudica* leaves and coffee powder.

Scanning Electron Microscopy (SEM) and Transmission Electron Microscopy (TEM). The morphological study of the green synthesized zinc oxide nanoparticles was performed by SEM.⁴² The particles show semispherical shape,

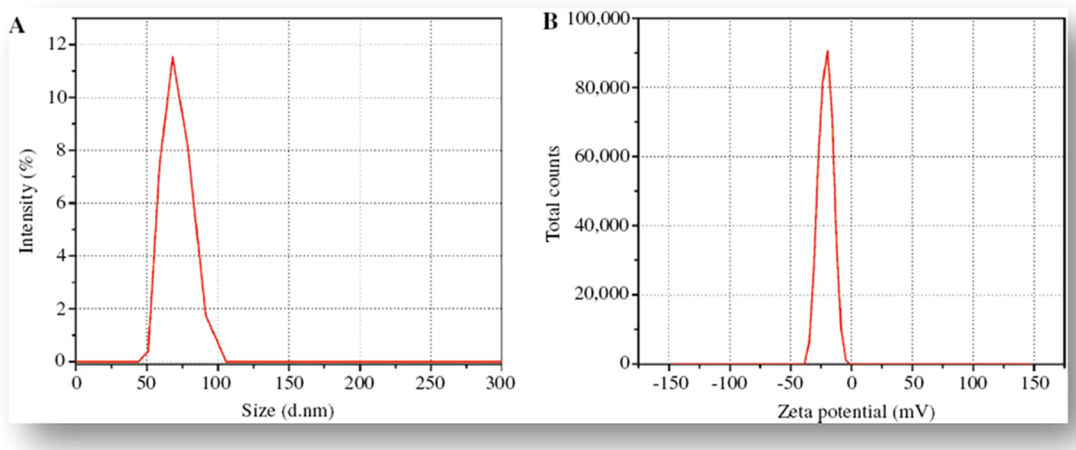


Figure 3. (A) Size distribution potential and (B) ζ -potential distribution of *M. fragrans* fruit-synthesized ZnO-NPs.

Table 1. Antibacterial Activity of *M. fragrans* Fruit-Synthesized ZnO-NPs

test organisms	activity of ZnO-NPs	antibiotics	CLSI standard	ZnO-NPs	antibiotic-coated ZnO-NPs	increase in the potency of coated ZnO-NPs
<i>E. coli</i>	15 \pm 1.54	ciprofloxacin	21	17.3 \pm 1.3	24.3 \pm 1.2	32.2
		imipinem	22	19 \pm 0.8	25 \pm 0.87	27.3
		vancomycin	19	11 \pm 1.1	14 \pm 1.3	15.8
		amoxicillin-clavulanic acid	18	10 \pm 1.2	14.6 \pm 0.9	22.2
<i>K. pneumoniae</i>	27 \pm 1.73	ciprofloxacin	21	16.3 \pm 0.7	25.6 \pm 1.4	41.4
		imipinem	22	19 \pm 0.8	26 \pm 1.5	31.8
		vancomycin	19	10 \pm 1.1	13 \pm 0.3	15.8
		amoxicillin-clavulanic acid	18	10.3 \pm 0.4	14.6 \pm 1.4	23.9
<i>P. aeruginosa</i>	17 \pm 1.66	ciprofloxacin	21	15.6 \pm 0.7	23 \pm 1.4	35.3
		imipinem	22	20 \pm 0.8	25.3 \pm 1.5	24.1
		vancomycin	19	8 \pm 1.1	10 \pm 0.3	10.5
		amoxicillin-clavulanic acid	18	15.6 \pm 0.4	18.6 \pm 1.4	11.2
<i>S. aureus</i>	21 \pm 1.73	ciprofloxacin	21	14.3 \pm 0.7	26 \pm 1.4	55.8
		imipinem	22	20 \pm 0.8	26.6 \pm 1.5	30.0
		vancomycin	19	8 \pm 1.1	18.6 \pm 0.3	55.7
		amoxicillin-clavulanic acid	18	10 \pm 0.4	12.3 \pm 1.4	12.8

200 and these particles are in a highly agglomerated form, as shown
201 in Figure 2A. This clearly shows that the particles are present
202 in a homogeneous form and the homogeneity of nanoparticles
203 plays important roles in their different activities. The particle
204 size ranged from 43.3 to 83.1 nm, respectively. The size
205 increase was due to the overlapping of particles on each other.
206 The morphology and particle size of pure zinc oxide
207 nanoparticles were observed using TEM micrographs, as
208 shown in Figure 2B. The presence of spherical- to
209 hexagonal-shaped particles with a grain size of 35.5 nm was
210 observed. We confirm the formation of ZnO-NPs by
211 comparing the particle size obtained from X-ray diffraction
212 and transmission electron microscopy. Our results are in
213 harmony with previous reports.⁴³

214 **Energy-Dispersive X-ray Analysis (EDX).** The EDX of
215 the NPs reveals that there is clearly the formation of zinc oxide
216 nanoparticles. The atomic weight of oxygen was 48.83%, while
217 its weight present was 21%. On the other hand, the atomic
218 weight of zinc was 37.16%, while its weight present was
219 65.35%, while the other minor constituents present in the

ZnO-NPs were due to the presence of the root extract of 220
ganger, as shown in Figure 2C. 221

222 **ζ -Potential.** The size distribution and ζ -potential of the 223
biosynthesized ZnO-NPs were investigated using the dynamic 224
light scattering (DLS) technique. The ζ -potential defines the 225
colloidal stability and is a typical measurement of the surface 226
charge on a particle. Suspensions that exhibit 15 mV are 227
generalized as stable colloids.⁴⁴ In the study, the ζ -potential of 227
the ZnO-NPs in distilled water (DW) was measured as -22.1 228
mV, and this can thus be considered as strongly anionic. The ζ - 229
potential measurements thus verify and support the dispersion 230
capacity of the greenly synthesized ZnO-NPs. The negative 231
surface charge is due to the binding affinity of extract 232
compounds with the NPs, conferring stability of the zinc 233
oxide nanoparticles and alleviating the aggregation potential of 234
the particles.⁴⁵ The hydrodynamic size of the particles was 235
determined using dynamic light scattering and was found to be 236
66 nm for the aqueous preparation of ZnO-NPs, as shown in 237
Figure 3A. The size distribution graph shows that the particle 238
size is polydispersed and larger compared to that obtained 239
from SEM observations. The increased size of the ZnO-NPs 240

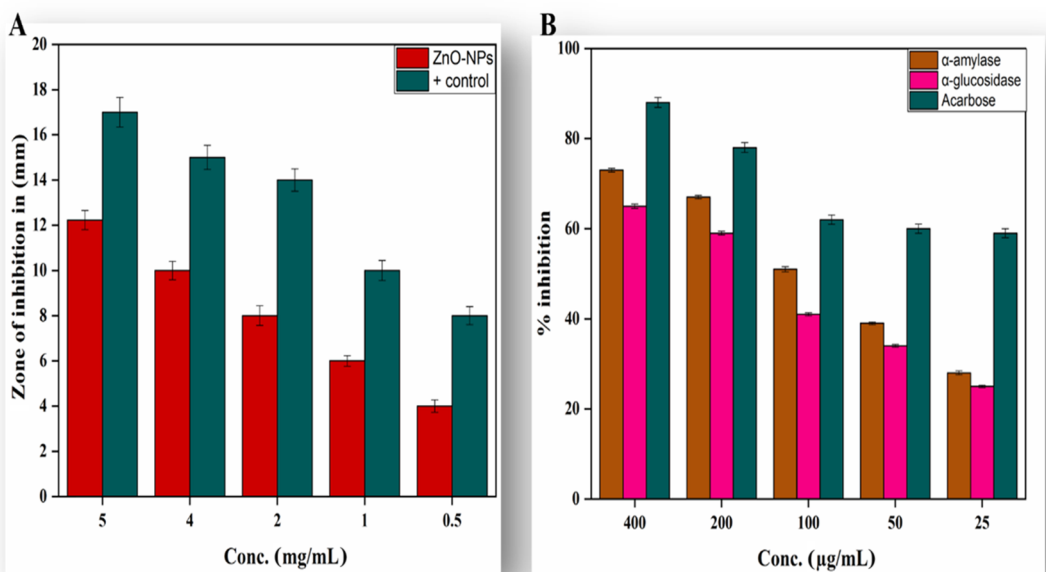


Figure 4. (A) Protein kinase inhibition and (B) antidiabetic activity of synthesized ZnO-NPs.

241 measured via DLS is due to the bias of the technique toward
 242 the measurement of larger particles (or even aggregates).⁴⁴
 243 Different functional groups (carbohydrates, polysaccharides,
 244 pectin, etc.) present in plant extract adsorbed on the surface of
 245 the NPs may affect its ζ -potential. There is a close relationship
 246 between these metabolites absorbed on the surface of ZnO-
 247 NPs and ζ -potential.⁴⁶

248 ■ BIOLOGICAL APPLICATIONS

249 **Antibacterial Assay.** Antibiotic resistance is a major
 250 problem that continues to plague a broad part of the world's
 251 healthcare system of both developing and developed countries.
 252 Current antibacterial therapy has been significantly influenced
 253 by the rise and proliferation of multidrug-resistant infections. A
 254 quest for a new supply of antimicrobials such as plant-mediated
 255 nanomaterials was included, as they possess a variety of
 256 bioactive compounds with proven therapeutic properties.^{47–49}
 257 In the present scenario, environmentally sustainable methods
 258 for synthesizing metallic nanoparticles have become a
 259 beneficial development. The use of plant extract phytochem-
 260 icals has become a specific nanoparticle synthesis technique, as
 261 they impart a dual role of reducing and capping agents to the
 262 nanoparticles. We synthesized ZnO-NPs using a common
 263 medicinal plant in the current study and tested their
 264 antibacterial efficacy against UTI bacterial strains.⁵⁰ Table 1
 265 depicts the complete profile of antibacterial activity of ZnO-
 266 NPs and noncoated and ZnO-NP-coated antibiotics against
 267 test organisms. In the current study, it was observed that 1%
 268 ZnO-NP solution (1 mg/mL dimethyl sulfoxide (DMSO)
 269 solution) displayed maximum zone of inhibition against
 270 *Klebsiella pneumoniae* (27 ± 1.73 mm), *Escherichia coli* ($15 \pm$
 271 1.54 mm), *Pseudomonas aeruginosa* (17 ± 1.66 mm), and
 272 *Staphylococcus aureus* (21 ± 1.73 mm). However, it was
 273 perceived that *E. coli*, *K. pneumoniae*, *P. aeruginosa*, and *S.*
 274 *aureus* displayed resistance patterns against noncoated
 275 ciprofloxacin, imipinem, vancomycin, and amoxicillin-clav-
 276 ulanic acid antibiotics. On the other hand, the activity of
 277 antibiotics increased significantly against these strains after
 278 being coated with ZnO-NPs. It was observed that the activity

ZnO-NP-coated ciprofloxacin, imipinem, vancomycin, and
 279 amoxicillin-clavulanic acid antibiotics increased up to 32.2,
 280 27.3, 15.8, and 22.2% against *E. coli*; up to 41.4, 31.8, 15.8, and
 281 23.9% against *K. pneumoniae*; up to 35.3, 24.1, 10.5, and 11.2%
 282 against *P. aeruginosa*; and up to 55.8, 30, 55.7, and 12.8%
 283 against *S. aureus*, respectively. Our results are in resemblance
 284 with previous studies.^{51,52} 285

Protein Kinase Inhibition Assay. Protein kinase enzymes
 286 play a substantial role in anticancer studies. These enzymes
 287 have the ability to phosphorylate tyrosine and serine–
 288 threonine amino acid residues that are necessary for running
 289 certain important cellular pathways like differentiation,
 290 proliferation, and cell death.⁵³ Uncontrolled phosphorylation
 291 caused by protein kinase enzyme produces factors that can lead
 292 to tumor growth, and entities with the potential to deter these
 293 enzymes are of significant importance in anticancer research.⁵⁴
 294 Streptomyces 8SE strain was used to elucidate the protein
 295 kinase inhibition capability of biogenic ZnO-NPs. Clear zones
 296 were observed against each tested concentration of tested
 297 ZnO-NPs. The largest bald zone of 12.23 ± 0.42 mm at 5 mg/
 298 mL and the smallest bald zone of 4.91 ± 0.17 mm were
 299 observed at 500 μ g/mL. Our results are in accordance with the
 300 literature available on ZnO-NP kinase inhibition enzymes.⁵⁵
 301 Overall results concluded that the biogenic NPs acquire vital
 302 capping and stabilizing agents from plant extracts responsible
 303 for anticancerous capability. Biogenic ZnO-NPs were observed
 304 to inhibit Streptomyces strain in a dose-dependent manner, as
 305 shown in Figure 4A. 306 f4

Antidiabetic Activity. Diabetes mellitus (DM) is a
 307 metabolic condition characterized by chronic hyperglycemia
 308 due to reduced insulin production or insensitivity of body cells
 309 to insulin that has already been produced.⁵⁶ There were 425
 310 million people living with DM, according to the International
 311 Diabetes Federation (IDF) survey for 2017, and this number
 312 will increase to 629 million by 2045.⁵⁷ One effective clinical
 313 strategy for the treatment of DM is the reduction of
 314 postprandial hyperglycemia, which can be done by inhibiting
 315 α amylase and α glucosidase, the two most important
 316 carbohydrate hydrolyzing enzymes in the digestive tract.⁵⁶ A
 317

Table 2. Antioxidizing Potential of Synthesized ZnO-NPs

conc ($\mu\text{g/mL}$)	TAC ($\mu\text{g AAE/mL}$)	TRP ($\mu\text{g AAE/mL}$)	ABTS (TEAC)	DPPH (%FRSA)
400	71.1 \pm 0.83	63.41 \pm 0.83	82.12 \pm 0.28	66.3 \pm 0.28
200	62.37 \pm 0.27	57.51 \pm 0.87	74.63 \pm 0.39	51.1 \pm 0.71
100	54.86 \pm 0.72	43.23 \pm 0.26	67.64 \pm 0.56	37.69 \pm 0.32
50	35.29 \pm 0.76	27.76 \pm 0.58	55.47 \pm 0.26	28.45 \pm 0.98
25	29.16 \pm 0.25	17.41 \pm 0.36	40.39 \pm 0.15	20.19 \pm 0.48

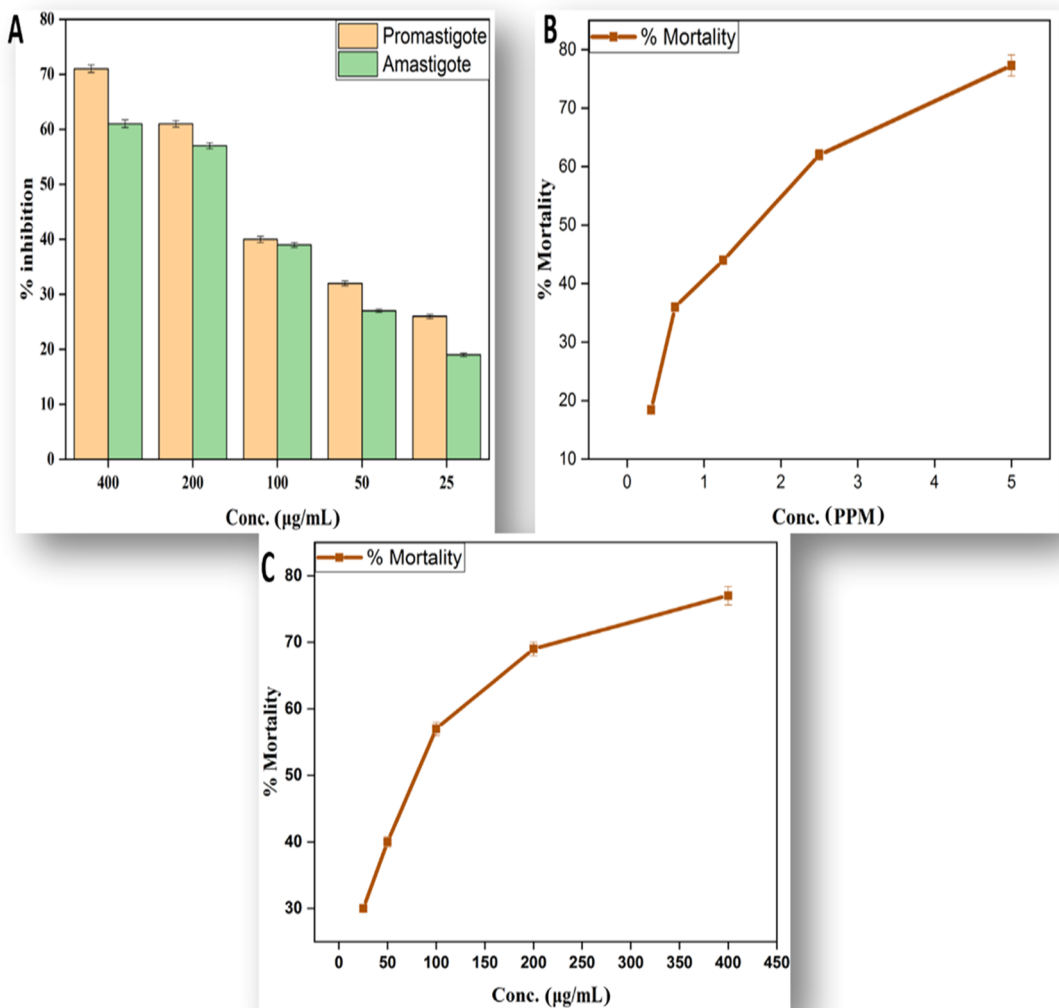


Figure 5. (A) %Mortality of amastigote and promastigote, (B) antilarvical activity, and (C) brine shrimps' lethality assay of ZnO-NPs.

point of enormous importance is the search for new sources of natural products with probable antidiabetic action from tropical flora and nanotools. In this study, nanoparticle samples of zinc oxide NPs were evaluated for α -amylase and α -glucosidase inhibition, as shown in Figure 4B. Our findings indicated excellent α -amylase and α -glucosidase inhibition activity. Maximum inhibition of about 73.23 ± 0.42 for α -amylase and 65.21 ± 0.49 for α -glucosidase was calculated at 400 $\mu\text{g/mL}$. Our results are in agreement with a previous report conducted on several classes on NPs.^{58,59} Here, we show that biobased nanoparticles can exhibit tremendous antidiabetic behavior and are considered to be an effective therapeutic agent for the treatment of diabetes as an alternative to the use of costly and less efficient drugs.

Antioxidant Assay. The change in plant metabolic pathways is attributed to environmental stress that results in reactive oxygen species (ROS) destroying membrane lipids, plant cells, DNA, and proteins.⁶⁰ Many metabolically important compounds like flavonoids, terpenoids, and oxidative stress-responsive agents play a promising role in the capping and stabilization of the nanoparticles.^{61,62} Four separate assays, i.e., total antioxidant capacity (TAC), total reduction power (TRP), 2,2'-azino-bis(3-ethylbenzothiazoline-6-sulfonic acid) (ABTS), and 2,2-diphenyl-1-picrylhydrazyl (DPPH) free radical scavenging assay (FRSA), were conducted to assess the *in vitro* antioxidant potential of plant-synthesized NPs. We summarize the phosphomolbdenum-based technique to find the dose-dependent antioxidant potential of biogenic ZnO-NPs. This technique is based on the

347 reduction of Mo(VI) to Mo(V) with the help of an antioxidant
348 mediator that results in the formation of phosphate-molybdate,
349 and the color of phosphate-molybdate is green, which helps in
350 its identification.^{63,64} Antioxidant capacity of biogenic ZnO-
351 NPs in comparison to that of ascorbic acid is recorded to be
352 $71.1 \pm 0.83 \mu\text{g AAE/mg}$ at $400 \mu\text{g/mL}$. Total antioxidant
353 capacity (TAC) was amplified with the total reducing power
354 estimation (TRP) assay. If the tested sample possesses redox
355 potential, it will convert the Fe^{+3} to Fe^{+2} ion.⁶⁵ Like TAC, the
356 highest TRP was noted as 63.41 ± 0.83 at the highest tested
357 concentration. Furthermore, to support the TAC and TRP
358 findings, ABTS (2,2'-azino-bis(3-ethylbenzothiazoline-6-sul-
359 fonic acid)) and DPPH (2,2-diphenyl-1-picrylhydrazyl) free
360 radical scavenging assays were also performed. DPPH is a
361 stable free radical that is reduced by accepting hydrogen or
362 electron from a donor based on formation of a yellowish
363 diphenyl picrylhydrazine molecule.⁶⁶ These spectrophotometric-
364 ric methods are based on quenching of stable colored radicals
365 of DPPH and ABTS, indicating the scavenging ability of the
366 antioxidant sample. In the study, excellent free radical
367 scavenging activity of all test concentrations was revealed, as
368 summarized in Table 2. The highest DPPH and ABTS free
369 radical scavenging activities at $400 \mu\text{g/mL}$ were noted as 66.3
370 ± 0.28 and 82.12 ± 0.28 TEAC for ZnO-NPs, respectively. All
371 of these assays were carried out in triplicates, and the values
372 were recorded as means of their triplicates. Our results are in
373 harmony with previous reports.^{50,67}

374 **Antileishmanial Assay.** Leishmaniasis is a severe, non-
375 contagious, infectious disease caused mainly by parasites
376 present in the genus *Leishmania*. Leishmaniasis is one of the
377 six major infectious diseases in tropical and subtropical
378 countries, with a mortality rate of 50 000 deaths per year,
379 according to the World Health Organization (WHO).⁶⁸ The
380 disease is at high risk of unregulated dissemination due to
381 inadequate vectors and inefficient and inexpensive medicines.
382 Metal oxide nanoparticle (zinc, silver, titanium, and
383 magnesium oxide)-related therapies have recently become
384 common due to their strong cytotoxic ability toward
385 *Leishmania*.⁶⁹ We use different concentrations of the biogenic
386 ZnO-NPs from 25 to $400 \mu\text{g/mL}$ for finding out their
387 antileishmanial activity against amastigotes and promastigotes
388 using the 3-(4,5-dimethylthiazol-2-yl)-2,5-diphenyltetrazolium
389 bromide (MTT) assay, as illustrated in Figure 5A. At the
390 highest concentration of $400 \mu\text{g/mL}$, the biogenic NPs possess
391 the potent mortality rate of 71.50 ± 0.70 for promastigotes and
392 61.41 ± 0.71 for amastigotes. The lowest mortality rate
393 recorded for biogenic ZnO-NPs was 26.90 ± 0.39 for
394 promastigote and 19.60 ± 0.33 for amastigote. The results of
395 our study are in agreement with previous studies.^{28,70}

396 **Antilarvicidal Activity.** In recent decades, the prevalence
397 of dengue has risen significantly around the world. About 2.5
398 billion people, two-fifths of the world's population, are already
399 at risk from dengue. The WHO currently predicts that there
400 could be 50 million dengue infections worldwide per year.⁷¹
401 *Aedes aegypti* L., a dengue vector carrying the liable arbovirus,
402 is commonly spread in the tropical and subtropical areas in
403 recent times. Fighting the disease-carrying mosquitoes is the
404 best way to avoid the dengue virus spread.⁷² Material scientists
405 in recent times are more focused to find better alternatives
406 using plant extracts and plant-mediated NPs against the
407 proposed vector. In the present study, a range of concentrations
408 of synthesized NPs (0.3125, 0.6250, 1.25, 2.5, 5 ppm) were
409 tested against the second and fourth instars of *A. aegypti*. In

410 total, $77.3 \pm 1.8\%$ mortality was observed at 5 ppm followed
411 by $18.4 \pm 0.44\%$ at 0.3125 ppm, as shown in Figure 5B. At
412 subsequently reduced concentrations, mortality reduced in
413

414 **Brine Shrimp Lethality Assay.** In recent years, the role of
415 brine shrimp in aquaculture has become important. In winter,
416 about 10 million pounds of brine shrimp eggs are harvested
417 and marketed as food for tropical fish.⁷³ *Artemia* is an
418 appropriate organism for research of bioassays and toxicity. In
419 the aquatic food chain, this species has a central function.⁷⁴
420 The main aim of our study is to find the acute toxicities of
421 ZnO-NPs. Concentrations are applied in a higher dose manner
422 from 25 to $400 \mu\text{g/mL}$. The highest mortality value of 77 ± 1.4
423 is observed at $400 \mu\text{g/mL}$. The toxicity pattern of metallic NPs
424 toward *Artemia salina* is dose-dependent. The lowest value of
425 30 ± 0.44 is observed at $25 \mu\text{g/mL}$, as shown in Figure 5C.
426 The results of NPs themselves, dissolution products, and
427 agglomerates of NPs formed during the experiment can result
428 in toxicity of NPs. The findings of this analysis showed that
429 proper consideration should be paid to the possible eco-
430 toxicity and environmental health consequences of NPs.^{75,76}

431 **In Vitro Biocompatibility Studies.** For the demonstration
432 of the biocompatibility of the green synthesized NPs, a
433 biocompatibility assay was performed using human red blood
434 cells. In this bioassay, hemolysis of the human red blood cells is
435 noted against various concentrations of the nanoparticles (25–
436 $400 \mu\text{g/mL}$). Hemolysis of RBCs is measured at 405 nm using
437 a spectrophotometer. The hemolysis of RBCs will only be
438 observed if the sample has the ability to rupture the cells. The
439 biocompatibility results of our study are listed in Table 3. The
440 t3

Table 3. % Hemolysis of Green Synthesized ZnO-NPs

Sl no.	conc. ($\mu\text{g/mL}$)	% hemolysis
1	400	3.58 ± 0.11
2	200	2.46 ± 0.14
3	100	0.97 ± 0.09
4	50	0.53 ± 0.06

441 American Society for Testing Materials has issued some
442 guidelines for biocompatibility of substances, and according to
443 that guidelines, substances having $>2\%$ hemolysis are labeled as
444 nonhemolytic, 2–5% slightly hemolytic, and $>5\%$ are
445 considered as hemolytic.⁷⁷ As can be seen from Table 3, all
446 our stock solutions of synthesized nanoparticles show less
447 hemolysis even at high concentrations, which shows their high
448 biocompatibility. To use NPs for biomedical applications, we
449 have to check their biocompatibility. Our biogenic ZnO-NPs
450 are hem-compatible, and even at a high concentration of 400
451 $\mu\text{g/mL}$, we observed no hemolytic activity. The biocompat-
452 ility results of our study thus show that plant-based
453 synthesized nanoparticles are biosafe and we can use ZnO-
454 NPs for therapeutic purposes.

■ PHOTOCATALYTIC ACTIVITIES OF ZN-NPS FOR THE DEGRADATION OF METHYLENE BLUE DYE

455 **Effect of Irradiation Time.** With an increase of UV light
456 illumination in the initial 20 min, the degradation was observed
457 at 19.6%, while with a further increase in time, the degradation
458 of dye also increased and the maximum degradation was
459 observed at 140 min, which was 88%, as shown in Figure 6a,b.
460 f6

461 **Mechanism of Photocatalytic Catalytic Degradation
of the Dye.** We have already studied the relationship between
462

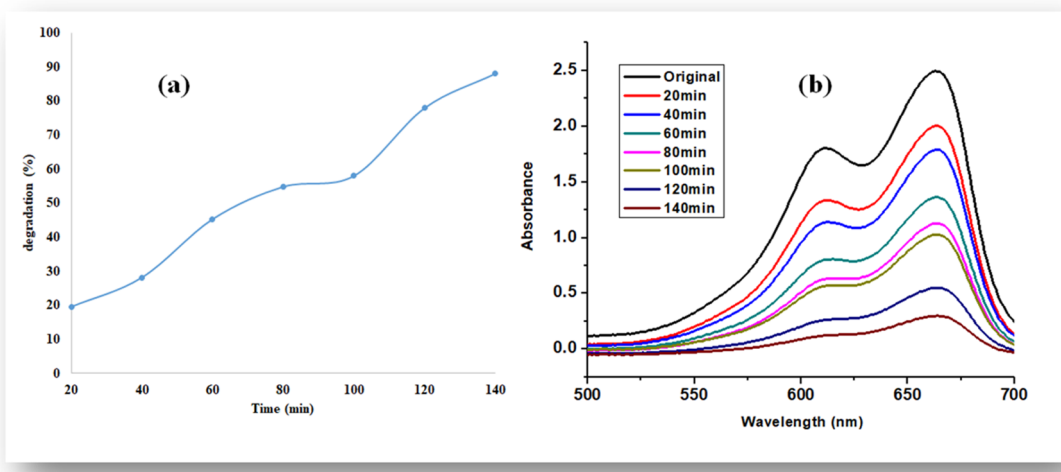
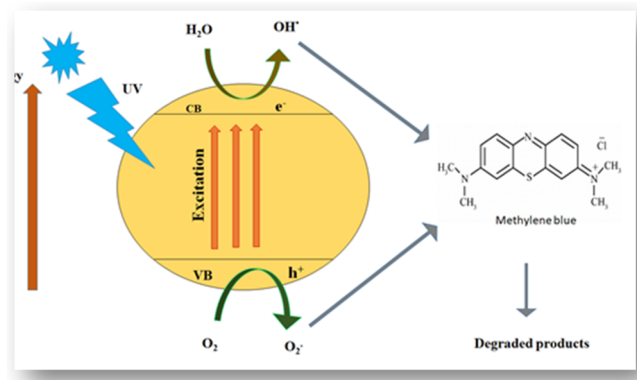


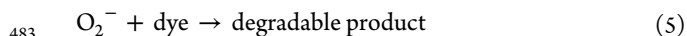
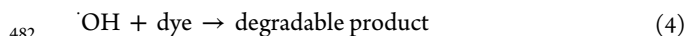
Figure 6. (a) Percent degradation of methylene blue dye with ZnO nanoparticles and (b) UV-visible spectra.

463 the time and the degradation process; now, we need to know
 464 how this degradation process happens. The effect of time on
 465 the degradation process was studied to know the mechanism.⁷⁸
 466 The light-dependent degradation process of methylene blue
 467 dye is illustrated in Scheme 1. First, the dye is adsorbed on the

Scheme 1. Reaction Mechanism for the Degradation of Methylene Blue



468 surface of the catalyst (zinc in this case) and then it is exposed
 469 to ultraviolet light illumination to excite valence electrons so
 470 the electrons may transfer to the conduction band from the
 471 valence band; during the process, a positive hole h⁺ is lifted
 472 inside the valence band. The positive holes and free electrons
 473 will react on the surface of the photocatalyst along with
 474 adsorbed water molecules, and as a result, the positive holes
 475 will react with water to produce OH⁻ radicals and the free
 476 electrons reduce the dissolved oxygen to superoxide anion
 477 O₂^{•-} radicals. These light-generated radicals degrade the dye
 478 molecules into simple molecules such as CO₂ and H₂O.⁷⁹



CONCLUSIONS

This research work is basically focused on one-pot eco-friendly plant-based synthesis of biomedically important ZnO-NPs using aqueous fruit extracts of *M. fragrans*, a medicinally important plant. XRD analysis has verified the crystalline structure of the synthesized NPs. Fourier transform infrared (FTIR) spectroscopy analysis verified the existence of phytochemicals involved in the transfer of metallic ions to NPs. Morphologies and vibrational modes were determined by SEM and TEM analyses, DLS determined the surface charge and stability, and also the stability is determined by TGA. Synthesized ZnO-NPs have shown successful capacity for antioxidants and against bacterial strains. There is moderate inhibitory ability for bioengineered ZnO-NPs against α -amylase and α -glucosidase enzymes. Biogenic ZnO-NPs were found to have significant potency against brine shrimps and larvae of *A. aegypti*. The synthesized ZnO-NPs were also effective in the degradation of methylene blue dye. Synthesized ZnO-NPs were also documented to be biocompatible with human red blood cells. Our research work concluded that the above-mentioned biogenic ZnO-NPs can be used for different studies in diseases, cosmetics, and cancers. More research on zinc oxide nanoparticles is needed to explore their applications in biomedicine at both *in vitro* and *in vivo* levels.

METHODS

Plant Collection and Extraction. *M. fragrans* fruits were purchased from a local market in Pakistan. The plant material was converted into fine powder through an electric grinder for the preparation of extracts. The plant powder (50 g) was soaked in 500 mL of distilled water and heated at 150 °C for 20 min. For maximum extraction, the soaked powder was kept in an incubator at 37 °C overnight. The extract was filtered through Whatman filter paper no. 1823, and then, the solvent was evaporated through a rotatory evaporator at 40 °C. The obtained extract was preserved in a refrigerator at 4 °C.

Synthesis of ZnO-NPs. Zinc oxide nanoparticles were synthesized according to a previously described protocol with slight modifications. Briefly, 6.0 g of zinc acetate dihydrate (Zn(NO₃)₂·2H₂O) (Sigma-Aldrich) was added to 100 mL of extract and kept on a magnetic stirrer at 60 °C for 2 h. Once the reaction was complete, the mixture was allowed to cool down at 25 °C and centrifuged (HERMLE Z326K) at 10 000 × g.

526 rpm for 10 min. The supernatant was discarded, and the 527 remaining pellet was washed thrice with distilled water, poured 528 into a clean Petri plate, and oven-dried at 90 °C. The dried 529 material was then ground into fine powder in a pestle and 530 mortar and calcined for 2 h at 500 °C to remove any 531 impurities. The annealed powder was stored in an airtight glass 532 vial, labeled as ZnO-NPs, and was further used for physical 533 characterizations and biological applications.²⁸

534 **Characterization of Biosynthesized ZnO-NPs.** To 535 analyze the physicochemical properties of ZnO-NPs, different 536 characterization techniques have been used to analyze the 537 physicochemical properties of ZnO-NPs synthesized from *M. 538 fragrans*. These techniques include UV spectroscopy, Fourier 539 transform infrared (FTIR) spectroscopy, X-ray diffraction 540 (XRD), scanning electron microscopy (SEM), transmission 541 electron microscopy (TEM), energy-dispersive X-ray (EDX) 542 analysis, dynamic light scattering (DLS), and thermogravimetric 543 analysis (TGA).

544 The reaction carried out between the extract and zinc nitrate 545 solution was analyzed using UV-visible spectroscopy in the 546 range of 200–700 nm. To detect the nature of green 547 synthesized zinc oxide nanoparticles, the X-ray diffraction 548 technique was used. A PANalytica X'pert X-ray diffractometer 549 was used to obtain the X-ray diffraction pattern. For finding the 550 size of the crystallite, we use Scherer's equation⁸⁰

$$D = k\lambda/\beta \cos \theta$$

551 where D represents the half peak height of an XRD line due to 552 a specific crystalline plane, k denotes the shape factor (0.94), λ 553 depicts the X-ray wavelength of 1.5421 Å, and β and θ refer to 554 FWHM in radian and Bragg's angle, respectively. The 555 functional group responsible for the formulation of nano- 556 particles was detected using Fourier transform infrared (FTIR) 557 spectroscopy in the spectral range of 400 and 4000 cm^{-1} . 558 Morphologies and physical dimensions were examined by SEM 559 (JSM-7600F, Japan) and TEM (JEM-2100F, Japan), while 560 elemental analysis was conducted using energy-dispersive X-ray 561 spectroscopy (EDX).⁸¹

562 The electrostatic potential that occurs at the shear plane of a 563 particle, which is of concern to both the surface charge and the 564 local medium of the particle is known as ζ -potential. We 565 analyze the ζ -potential using a zeta potential analyzer. We use 566 phase analysis light scattering mode and maintain proper room 567 temperature for recording all of the measurements. For the 568 calculation of the ζ -potential, we use the Smoluchowski 569 equation mentioned below.

$$v = (\varepsilon E/\eta) \xi$$

570 where v = electrophoretic velocity, η = viscosity, ε = electrical 571 permittivity of the electrolytic solution, and E = electric field.⁸²

572 Thermogravimetric analysis was carried out using a Q500 573 thermogravimetric analyzer for the investigation of thermal 574 stability. For the above purpose, 5 mg of the tested sample was 575 decomposed under flowing nitrogen gas from 30 to 600 °C at 576 10 °C/min heating rate.

577 ■ BIOLOGICAL APPLICATIONS

578 **Antibacterial Activities. Bacterial Species Collection.** 579 Overall, four MDR strains *K. pneumoniae*, *E. coli*, *P. aeruginosa*, 580 and *S. aureus* were analyzed for confirmation of antibacterial 581 activity. The strains were already isolated from patients with 582 urinary tract infections. All of these isolates were collected 583 from Hayat Abad Medical Complex Peshawar (HMC),

584 Pakistan. Biochemical and molecular tests (16S RNA) were 585 done at the hospital for the identification of these UTI isolates. 585

586 **ZnO-NP-Coated Antibiotic Disc Preparation.** Zinc oxide 587 nanoparticle residues (20 mg) were mixed with 1 mL of 587 distilled water to prepare the stock solution of powdered ZnO- 588 NPs. After complete mixing, we take 5 μL from the prepared 589 stock solution, poured it on the antibiotic disc, and placed the 590 disc inside the oven for drying at 80 °C and for 15 min. The 591 same procedure was used for each antibiotic. 592

593 **Agar Well Diffusion Assay for ZnO-NPs.** The wells, having 594 8 mm diameter, were punched into the nutrient agar (NA) 594 media followed by bacterial lawn preparation in the media.⁸³ 595 The wells were filled with 100 μL of ZnO-NP suspension. The 596 Petri dishes were then kept in an incubator at 37 °C for 24 h. 597 Just after the incubation, the potency of ZnO-NPs against the 598 tested MDR bacterial strains was determined by measuring 599 zones of inhibition in millimeters. 600

601 **Disc Diffusion Assay for Antibiotic Discs and Antibiotic- 602 Coated ZnO-NPs.** To evaluate the potency of both coated and 602 noncoated antibiotics against tested MDR bacterial strains, the 603 standard Kirby Bauer disc method was used. Nutrient agar was 604 prepared, and then, NA media along with Petri dishes were 605 autoclaved using standard SOPs. After the medium was 606 sterilized, it was cooled to 50 °C and then poured into 607 sterilized Petri dishes in a biosafety cabinet. After the media 608 were solidified, bacterial lawns were prepared on nutrient agar 609 (NA) plates, then both ZnO-NP-coated and noncoated 610 antibiotic discs were applied, and the Petri plates were 611 incubated at 37 °C for 24 h. After incubation, the potency 612 of both coated and noncoated antibiotics against test MDR 613 bacterial strains was determined by measuring zones of 614 inhibition in millimeters. 615

616 **Protein Kinase Inhibition Assay.** For screening the 617 anticancer activity of biosynthesized ZnO-NPs, a protein 618 kinase inhibition assay was performed. This is a preliminary 618 bioassay for the confirmation of the protein kinase inhibitory 619 ability of the synthesized NPs. Our protocol was slightly 620 different from that followed by ref 28. A test strain of 621 *Streptomyces 85E* was used. We prepare the plate containing 622 sterile ISP4 medium and then transferred a volume of 100 μL 623 from the refreshed culture of *Streptomyces 85E* to the plates. 624 About 5 μL of ZnO-NPs was poured inside each well (5 mm) 625 and labeled accordingly. Surfactin and DMSO worked as 626 positive and negative controls. After this, all of the plates were 627 subjected to incubation at 28 °C for 2 days. We observed clear 628 and bald zones around wells, indicating the inhibition of 629 phosphorylation, mycelia, and formation of spores. A Vernier 630 calliper was used for the measurement of the zones to the 631 nearest millimeter. The clear zones show the cytotoxic 632 potential of ZnO-NPs and death of the test strain. 633

634 **Antidiabetic Assay.** The antidiabetic activity of the 634 biogenic ZnO-NPs was determined using α -glucosidase and 635 α -amylase inhibition assays. 636

637 **α -Amylase Inhibition Assay.** For the evaluation of the α - 637 amylase inhibition assay of the biogenic ZnO-NPs, we used the 638 most acceptable protocol with some minor changes.⁸⁴ To 639 perform this assay, we used a 96-well microplate. Inside each 640 well, we poured phosphate buffer (15 μL), α -amylase (25 μL), 641 sample (10 μL), and starch (40 μL). After this, the plate was 642 subjected to incubation at 50 °C for 30 min. At last, 20 μL of 643 HCl solution and 90 μL of iodine were added to each well. For 644 negative control, we used DMSO, and for positive control, 645 acarbose was used, while the blank contained buffer solution 646

647 and starch instead of ZnO-NPs. A microplate photometer was
648 operated at 540 nm for the observing the sample absorbance
649 capacity. We calculated the percentage inhibition with the
650 following formula.

$$\begin{aligned} & \text{% enzyme inhibition} \\ &= \left(\frac{\text{Abs sample} - \text{Abs negative control}}{\text{Abs blank} - \text{Abs negative control}} \right) \times 100 \end{aligned}$$

651 **α -Glucosidase Inhibition Assay.** ZnO-NPs' antidiabetic
652 activity was demonstrated using the α -glucosidase inhibition
653 assay.⁸⁵ For dissolving α -glucosidase (*Saccharomyces cerevisiae*,
654 Sigma-Aldrich), 50 mL of phosphate buffer having pH 6.8 was
655 supplemented with 100 mg of bovine serum albumin. The
656 reaction mixture prepared using 10 μ L of tested sample,
657 phosphate buffer (490 μ L; pH 6.8), and *p*-nitrophenyl α -D-
658 glucopyranoside (5 mM; 250 μ L) was kept in an incubator at
659 37 °C for 5 min. α -Glucosidase (0.15 units/mL; 250 μ L) was
660 then introduced to samples followed by reincubation for 15
661 min at 37 °C. After terminating the reaction by adding 2 mL of
662 Na₂CO₃ (200 mM) solution, absorption spectra were recorded
663 using a UV-vis spectrophotometer at 400 nm. The assay is
664 based on the quantification of *p*-nitrophenol released from *p*-
665 nitrophenyl α -D-glucopyranoside. In the experiment, acarbose
666 was employed as the positive control, and the experiment was
667 repeated thrice.

$$\begin{aligned} & \text{% enzyme inhibition} \\ &= \left(\frac{\text{Abs sample} - \text{Abs negative control}}{\text{Abs blank} - \text{Abs negative control}} \right) \times 100 \end{aligned}$$

668 **Antioxidant Assays. Total Antioxidant Capacity Deter-
669 mination (TAC).** For examination of total antioxidant capacity,
670 the same assay was used as reported by ref 86. Eppendorf tubes
671 were filled with 100 μ L of sample using a micropipette. Then,
672 we added 900 mL of TAC reagent to Eppendorf tubes (0.6 M
673 sulfuric acid, 28 mM sodium phosphate, and 4 mM ammonium
674 molybdate, in 50 mL of dH₂O). The reaction mixture was then
675 incubated at 90 °C for 2 h in a water bath; after cooling the
676 samples, absorbance was recorded at 630 nm by a microplate
677 reader. The above-mentioned procedure was performed three
678 times; TAC was expressed as μ g ascorbic acid equivalent/mg
679 of sample.

680 **Total Reducing Power (TRP) Determination.** For finding
681 out the total reducing power (TRP), the same procedure was
682 followed as reported by ref 87. The Eppendorf tube already
683 containing 100 μ L of the test sample was filled with 400 μ L of
684 0.2 M phosphate buffer having pH 6.6 and potassium ferric
685 cyanide (1% w/v); after this, the tube containing all of these
686 samples was incubated in a water bath for 30 min at 55 °C.
687 After incubation, 400 μ L of trichloroacetic acid (10% w/v) was
688 added to each Eppendorf tube and the Eppendorf tube was
689 subjected to centrifugation for 10 min at a speed of 3000 rpm.
690 After centrifugation, the supernatant (140 μ L) obtained was
691 poured into wells of a 96-well plate, which already contained
692 60 μ L of ferric cyanide solution (0.1% w/v); using a microplate
693 reader at 630 nm, we then recorded the absorbance of the
694 sample. The procedure mentioned above was used for both
695 positive and negative controls.

696 **Free Radical Scavenging Assay (FRSA).** For finding the
697 free radical scavenging ability of the biosynthesized and eco-
698 friendly zinc oxide nanoparticles, we follow the same protocol

699 used by ref 84 with some modifications. ZnO-NPs' free radical
700 scavenging is their antioxidant potential and was investigated
701 using the DPPH reagent. The activity was recorded at both the
702 lowest (12.5 μ L) and highest (400 μ L) concentrations. First,
703 we poured the tested sample of concentration (10 μ L) inside
704 the wells of a 96-well plate and then added (190 μ L) DPPH
705 reagent to every well already containing the tested samples.
706 After this, the samples were subjected to incubation in the dark
707 at a temperature of 37 °C for 60 min. For FRSA, we used both
708 a positive control (ascorbic acid) and a negative control
709 (DMSO). For recording the absorbance rate of the sample, we
710 used a microplate photometer at 515 nm. Free radical
711 scavenging ability of the biogenic ZnO-NPs was determined
712 using the following equation
713

$$\text{%FRSA} = \left(1 - \frac{\text{Abs}}{\text{Abc}} \right) \times 100$$

714 Abc and Abs indicates the absorbances of the negative control
715 and sample, respectively.

716 **Trolox Antioxidant Assay (ABTS).** The ABTS assay was
717 used for finding the antioxidant activity of the biogenic ZnO-
718 NPs. First, we mixed potassium persulfate (2.45 mM) and 7
719 mM ABTS salt in equal concentrations and then incubated the
720 mixture at room temperature. After incubating the samples at
721 room temperature, the mixture prepared above from potassium
722 persulfate and ABTS salt were kept in the dark for 15 min. The
723 sample absorbance was recorded using a BioTek ELX800 at
724 734 nm. To perform the assay, we take both positive (Trolox
725 reagent) and negative (DMSO) controls. The process was
726 repeated three times, and antioxidant results were expressed as
727 TEAC.

728 **Antileishmanial Assay.** Biogenic ZnO-NPs were eval-
729 uated for their antileishmanial activity against both amastigotes
730 and promastigotes using the standard protocol described
731 previously.⁸⁸ *Leishmania tropica* KWH23 strain was used for
732 evaluating anti-leishmanial activity of the biogenic zinc oxide
733 nanoparticles; for this purpose, we incubated the culture of *L.*
734 *tropica* KWH23 strain in MI99 medium, which was already
735 supplemented with fetal bovine serum (FBS). First, we took 20
736 μ L of tested sample and poured it in a 96-well plate and then
737 we added 180 μ L of aliquot into the wells of the 96-well plate;
738 the aliquot was taken from the suspension culture (seeding
739 density 1×10^6 cells/mL). After this, we incubated the mixture
740 at room temperature (25 °C) for 72 h. We took Amphotericin
741 B as the positive control and DMSO (1%) in phosphate-
742 buffered saline (PBS) as the negative control. After the
743 incubation, we poured 20 μ L of MTT solution (4 mg/mL in
744 dH₂O) inside each well and again incubated the culture plate
745 for 4 h at room temperature (25 °C). A microplate reader was
746 used to record the absorbance of the samples at 540 nm. The
747 percent inhibition was calculated using the formula
748

$$\text{%inhibition} = \left[1 - \left\{ \frac{\text{absorbance of sample}}{\text{absorbance of control}} \right\} \right] \times 100$$

749 The sample was analyzed again using different concentrations,
750 and the process was repeated three times. The IC₅₀ values were
751 revealed using TableCurve 2D software v5. 01.

752 **Larvicidal Assay.** For finding out the larvicidal potential of
753 biogenic ZnO-NPs, the same protocol was used as proposed by
754 the World Health Organization.³⁶ For this assay, four
755 experimental groups and one control group were designed. A
756

755 plastic well containing 25 third instar larvae and 200 mL of 756 tested suspension was used for the experimental group, while 757 the same was done in distilled water for the control group. 758 Four technical replicates were designed for each group 759 containing 500 larvae per larvicidal assay simplified as (100 760 larvae per concentration \times 4 concentrations) + (100 larvae per 761 control group). This process was done for five. We provided 762 standard insectary condition "28 \pm 1 °C temperature, 80 \pm 763 10% relative humidity, and 12 h light/12 h darkness 764 photoperiod"; the purpose of the condition was to maintain 765 larvae while performing the bioassay. We provided no food for 766 24 h after beginning the bioassay; the purpose was to record 767 the mortality rate of the larvae during the bioassay. The 768 mortality was detected by the common technique by providing 769 stimulus to the larvae; if they did not respond or move slightly 770 but not vigorously, they were considered dead.⁸⁹

771 **Brine Shrimp Cytotoxicity.** This activity was accom- 772 plished to determine the cytotoxic effectiveness of ZnO-NPs.⁹⁰ 773 Purchased eggs of *A. salina* from Ocean Star International were 774 stocked at 28 °C. The eggs were allowed to hatch in 34 g/L 775 artificial seawater in a tray near a light source at 37 °C. Ten 776 fresh hatched nauplii were taken and transferred to each well. 777 Test samples (12.5–200 µg/mL) were poured into each well, 778 and the adjusted volume was 300 µL at this stage. The shrimps 779 were observed and counted under a magnifying lens, after a 780 complete 24 h of exposure. The TableCurve tool was used to 781 determine LD; the percentage was also determined for dead 782 shrimps using mathematical formulas. For observing the brine 783 shrimp, we used the following concentrations of biogenic ZnO- 784 NPs in ppm: 0.2, 0.3, 0.4, 0.5.

785 **Biocompatibility Study.** Biogenic ZnO-NPs' biocompat- 786 ability was demonstrated using fresh human red blood cells 787 (hRBCs).⁹¹ Blood samples (1 mL) were taken from healthy 788 individuals in ethylenediaminetetraacetic acid (EDTA) tubes 789 after permission of the individual. After collection of blood 790 samples, the samples were subjected to centrifugation for the 791 isolation of RBCs. After centrifugation, supernatant and pellet 792 were obtained; the supernatant was discarded, and the pellet 793 was collected after washing three times with PBS. For the 794 preparation of PBS–erythrocyte suspension, we mix 200 µL of 795 RBCs with 9.8 mL of PBS (pH 7.2). Then, the suspensions of 796 erythrocytes and green synthesized ZnO-NPs were mixed in 797 Eppendorf tubes. The Eppendorf tubes containing the mixture 798 of erythrocyte suspension and biogenic NPs were then 799 subjected to incubation for 1 h at 35 °C. Reaction mixtures 800 were centrifuged at 1000 rpm for 10 min followed by transfer 801 of 200 µL of supernatant to a 96-well plate; and hemoglobin 802 release absorption spectra were recorded at 540 nm. As a 803 control, Triton X-100 (0.5%) was used, while DMSO was 804 considered as a negative control. %hemolysis was calculated 805 using the following formula

$$\% \text{hemolysis} = \left(\frac{\text{sample Ab} - \text{negative control Ab}}{\text{positive control Ab} - \text{negative control Ab}} \right) \times 100$$

806 where Ab stands for the absorbance of the samples as recorded. 807 **Photocatalytic Activity.** To find out the photocatalytic 808 activity of the biogenic zinc oxide nanoparticles, we prepared 809 20 ppm of methylene blue dye in 50 mL of deionized water.⁹² 810 The original concentration (5 mL) was taken from the 811 solution, while the remaining solution of 25 mg (0.025 g) of 812 ZnO-NP catalyst was added to 45 mL of dye solution; for

813 maintaining the adsorption–desorption equilibrium, the 814 solution was placed in the dark for 20 min, then the solution 815 was subject to UV light, and the sample was taken after every 816 20 min. Centrifugation was performed at 10 000 rpm for 15 817 min to remove the catalyst from the samples; the degradation 818 of dye was studied by a UV–visible spectrophotometer. The 819 percent degradation of the degraded dye was calculated by the 820 following formula

$$\% = \frac{C_0 - C_t}{C_0} \times 100$$

$$\% = \frac{A_0 - A_t}{A_0} \times 100$$

821 where C_0 and A_0 are the initial concentrations of the dye and C_t 822 and A_t are the concentrations after a time interval.

■ AUTHOR INFORMATION

Corresponding Author

Shah Faisal – Department of Biotechnology, Bacha Khan University, Charsadda, KPK, Pakistan; orcid.org/0000-0001-5474-2622; Email: shahfaisal11495@gmail.com

Authors

Hasnain Jan – Department of Biotechnology, Bacha Khan University, Charsadda, KPK, Pakistan; Department of Biotechnology, Quaid-i-Azam University, Islamabad 45320, Pakistan

Sajjad Ali Shah – Department of Biotechnology, Bacha Khan University, Charsadda, KPK, Pakistan

Sumaira Shah – Department of Botany, Bacha Khan University, Charsadda, KPK, Pakistan

Adan Khan – Institute of Chemical Sciences, University of Peshawar, Peshawar, KPK, Pakistan

Muhammad Taj Akbar – Department of Microbiology, Abdul Wali Khan University, Mardan, KPK, Pakistan

Muhammad Rizwan – Center for Biotechnology and Microbiology, University of Swat, Mingora, KPK, Pakistan

Faheem Jan – Programmatic Management of Drug Resistant T.B. Unit, Ayub Teaching Hospital, Abbottabad, Pakistan

Wajid Ullah – Department of Chemistry, Bacha Khan University, Charsadda, KPK, Pakistan

Noreen Akhtar – Department of Microbiology, Khyber Medical University, Peshawar 25100, KPK, Pakistan

Aishma Khattak – Department of Bioinformatics, Shaheed Benazir Bhutto University, Peshawar, KPK, Pakistan

Suliman Syed – Department of Biotechnology, Bacha Khan University, Charsadda, KPK, Pakistan

Complete contact information is available at: <https://pubs.acs.org/10.1021/acsomega.1c00310>

Notes

The authors declare no competing financial interest.

■ ACKNOWLEDGMENTS

The authors are grateful to the Department of Biotechnology, Bacha Khan University, Pakistan for providing research facilities.

■ REFERENCES

- (1) Ramsden, J. *Nanotechnology: An Introduction*; William Andrew, 2016.

864 (2) Albrecht, M. A.; Evans, C. W.; Raston, C. L. Green chemistry 865 and the health implications of nanoparticles. *Green Chem.* **2006**, *8*, 866 417–432.

867 (3) Herlekar, M.; Barve, S.; Kumar, R. Plant-mediated green 868 synthesis of iron nanoparticles. *J. Nanopart.* **2014**, *2014*, No. 140614.

869 (4) Simonis, F.; Schilthuizen, S. *Nanotechnology; Innovation* 870 *Opportunities for Tomorrow's Defence*; TNO Science & Industry 871 Future Technology Center: The Netherlands, 2006.

872 (5) Iravani, S. Green synthesis of metal nanoparticles using plants. 873 *Green Chem.* **2011**, *13*, 2638–2650.

874 (6) Duan, H.; Wang, D.; Li, Y. Green chemistry for nanoparticle 875 synthesis. *Chem. Soc. Rev.* **2015**, *44*, 5778–5792.

876 (7) Bala, N.; Saha, S.; Chakraborty, M.; Maiti, M.; Das, S.; Basu, R.; 877 Nandy, P. Green synthesis of zinc oxide nanoparticles using Hibiscus 878 subdariffa leaf extract: effect of temperature on synthesis, anti- 879 bacterial activity and anti-diabetic activity. *RSC Adv.* **2015**, *5*, 4993– 880 5003.

881 (8) Hasan, S. A review on nanoparticles: their synthesis and types. 882 *Res. J. Recent Sci.* **2015**, *4*, 1–3.

883 (9) Barzinjy, A. A.; Hamad, S. M.; Aydin, S.; Ahmed, M. H.; 884 Hussain, F. H. Green and eco-friendly synthesis of Nickel oxide 885 nanoparticles and its photocatalytic activity for methyl orange 886 degradation. *J. Mater. Sci.: Mater. Electron.* **2020**, *31*, 11303–11316.

887 (10) Altavilla, C.; Ciliberto, E. In *Inorganic Nanoparticles: Synthesis, 888 Applications, and Perspectives. An Overview*; Altavilla, C.; Ciliberto, E., 889 Eds.; CRC Press: New York, 2011; pp 1–17.

890 (11) Al-Naamani, L.; Dobretsov, S.; Dutta, J. Chitosan-zinc oxide 891 nanoparticle composite coating for active food packaging applications. 892 *Innovative Food Sci. Emerging Technol.* **2016**, *38*, 231–237.

893 (12) Sankapal, B. R.; Gajare, H. B.; Karade, S. S.; Salunkhe, R. R.; 894 Dubal, D. P. Zinc oxide encapsulated carbon nanotube thin films for 895 energy storage applications. *Electrochim. Acta* **2016**, *192*, 377–384.

896 (13) Kumar, R.; Al-Dossary, O.; Kumar, G.; Umar, A. Zinc oxide 897 nanostructures for NO₂ gas–sensor applications: A review. *Nano- 898 Micro Lett.* **2015**, *7*, 97–120.

899 (14) Kumar, S. G.; Rao, K. K. Zinc oxide based photocatalysis: 900 tailoring surface-bulk structure and related interfacial charge carrier 901 dynamics for better environmental applications. *RSC Adv.* **2015**, *5*, 902 3306–3351.

903 (15) Hatamie, A.; Khan, A.; Golabi, M.; Turner, A. P.; Beni, V.; 904 Mak, W. C.; Sadollahkhani, A.; Alnoor, H.; Zargar, B.; Bano, S.; et al. 905 Zinc oxide nanostructure-modified textile and its application to 906 biosensing, photocatalysis, and as antibacterial material. *Langmuir* 907 **2015**, *31*, 10913–10921.

908 (16) Mishra, P. K.; Mishra, H.; Ekielski, A.; Talegaonkar, S.; Vaidya, 909 B. Zinc oxide nanoparticles: a promising nanomaterial for biomedical 910 applications. *Drug Discovery Today* **2017**, *22*, 1825–1834.

911 (17) Nagajyothi, P.; Cha, S. J.; Yang, I. J.; Sreekanth, T.; Kim, K. J.; 912 Shin, H. M. Antioxidant and anti-inflammatory activities of zinc oxide 913 nanoparticles synthesized using *Polygala tenuifolia* root extract. *J. 914 Photochem. Photobiol. B* **2015**, *146*, 10–17.

915 (18) Cai, X.; Luo, Y.; Zhang, W.; Du, D.; Lin, Y. pH-Sensitive ZnO 916 quantum dots–doxorubicin nanoparticles for lung cancer targeted 917 drug delivery. *ACS Appl. Mater. Interfaces* **2016**, *8*, 22442–22450.

918 (19) Gutha, Y.; Pathak, J. L.; Zhang, W.; Zhang, Y.; Jiao, X. 919 Antibacterial and wound healing properties of chitosan/poly (vinyl 920 alcohol)/zinc oxide beads (CS/PVA/ZnO). *Int. J. Biol. Macromol.* 921 **2017**, *103*, 234–241.

922 (20) Lai, L.; Zhao, C.; Su, M.; Li, X.; Liu, X.; Jiang, H.; Amatore, C.; 923 Wang, X. In vivo target bio-imaging of Alzheimer's disease by 924 fluorescent zinc oxide nanoclusters. *Biomater. Sci.* **2016**, *4*, 1085– 925 1091.

926 (21) Periasamy, G.; Karim, A.; Gibrelibanos, M.; Gebremedhin, G. 927 Nutmeg (*Myristica fragrans* Houtt.) Oils. In *Essential Oils in Food* 928 *Preservation, Flavor and Safety*; Elsevier, 2016; pp 607–616.

929 (22) Asgarpanah, J.; Kazemivash, N. Phytochemistry and pharmacological properties of *Myristica fragrans* Hoytt.: A review. *Afr. J. 930 Biotechnol.* **2012**, *11*, 12787–12793.

932 (23) Francis, S. K.; James, B.; Varughese, S.; Nair, M. S. Phytochemical investigation on *Myristica fragrans* stem bark. *Nat. Prod. Res.* **2019**, *33*, 1204–1208.

934 (24) Barzinjy, A. A.; Hamad, S. M.; Abdulrahman, A. F.; Biro, S. J.; 935 Ghafor, A. A. Biosynthesis, characterization and mechanism of 936 formation of ZnO nanoparticles using *Petroselinum crispum* leaf 937 extract. *Curr. Org. Synth.* **2020**, *17*, 558–566.

938 (25) Weil, A. T. Nutmeg as a narcotic. *Econ. Bot.* **1965**, *19*, 194– 939 217.

940 (26) Chiu, S.; Wang, T.; Belski, M.; Abourashed, E. A. HPLC- 941 guided isolation, purification and characterization of phenylpropanoid 942 and phenolic constituents of nutmeg kernel (*Myristica fragrans*) *Nat. Prod. Commun.* **2016** *11* 4 DOI: 10.1177/1934578X1601100416.

944 (27) Piras, A.; Rosa, A.; Marongiu, B.; Atzori, A.; Dessì, M. A.; 945 Falconieri, D.; Porcedda, S. Extraction and separation of volatile and 946 fixed oils from seeds of *Myristica fragrans* by supercritical CO₂: 947 Chemical composition and cytotoxic activity on Caco-2 cancer cells. *J. 948 Food Sci.* **2012**, *77*, C448–C453.

949 (28) Jan, H.; Shah, M.; Usman, H.; Khan, A.; Muhammad, Z.; Hano, 950 C.; Abbasi, B. H. Biogenic Synthesis and Characterization of 951 Antimicrobial and Anti-parasitic Zinc Oxide (ZnO) Nanoparticles 952 using Aqueous Extracts of the Himalayan Columbine (*Aquilegia 953 pubiflora*). *Front. Mater.* **2020**, *7*, No. 249.

954 (29) Guilger-Casagrande, M.; de Lima, R. Synthesis of Silver 955 Nanoparticles Mediated by Fungi: A Review. *Front. Bioeng. Biotechnol.* **2019**, *7*, No. 287.

957 (30) Davis, K.; Yarbrough, R.; Froeschle, M.; White, J.; Rathnayake, 958 H. Band gap engineered zinc oxide nanostructures via a sol–gel 959 synthesis of solvent driven shape-controlled crystal growth. *RSC Adv.* **2019**, *9*, 14638–14648.

961 (31) Chava, R. K.; Kang, M. Improving the photovoltaic conversion 962 efficiency of ZnO based dye sensitized solar cells by indium doping. *J. 963 Alloys Compd.* **2017**, *692*, 67–76.

964 (32) Fu, L.; Fu, Z. *Plectranthus amboinicus* leaf extract–assisted 965 biosynthesis of ZnO nanoparticles and their photocatalytic activity. *966 Ceram. Int.* **2015**, *41*, 2492–2496.

967 (33) Wang, F.-H.; Chang, C.-L. Effect of substrate temperature on 968 transparent conducting Al and F co-doped ZnO thin films prepared 969 by rf magnetron sputtering. *Appl. Surf. Sci.* **2016**, *370*, 83–91.

970 (34) Nimbalkar, A. R.; Patil, M. G. Synthesis of ZnO thin film by 971 sol–gel spin coating technique for H₂S gas sensing application. *Physica 972 B* **2017**, *527*, 7–15.

973 (35) Lu, J.; Batjikh, I.; Hurh, J.; Han, Y.; Ali, H.; Mathiyalagan, R.; 974 Ling, C.; Ahn, J. C.; Yang, D. C. Photocatalytic degradation of 975 methylene blue using biosynthesized zinc oxide nanoparticles from 976 bark extract of *Kalopanax septemlobus*. *Optik* **2019**, *182*, 980–985.

977 (36) Kim, W. J.; Soshnikova, V.; Markus, J.; Oh, K. H.; 978 Anandapadmanaban, G.; Mathiyalagan, R.; Perez, Z. E. J.; Kim, Y. 979 J.; Yang, D. C. Room temperature synthesis of germanium dioxide 980 nanorods and their in vitro photocatalytic application. *Optik* **2019**, *178*, 664–668.

982 (37) Zhou, J.; Zhao, F.; Wang, Y.; Zhang, Y.; Yang, L. Size- 983 controlled synthesis of ZnO nanoparticles and their photoluminescence 984 properties. *J. Lumin.* **2007**, *122*–123, 195–197.

985 (38) Khoshhesab, Z. M.; Sarfaraz, M.; Asadabad, M. A. Preparation 986 of ZnO nanostructures by chemical precipitation method. *Synth. 987 React. Inorg. Met.-Org. Nano-Met. Chem.* **2011**, *41*, 814–819.

988 (39) Kaskow, I.; Decyk, P.; Sobczak, I. The effect of copper and 989 silver on the properties of Au-ZnO catalyst and its activity in glycerol 990 oxidation. *Appl. Surf. Sci.* **2018**, *444*, 197–207.

991 (40) Arakha, M.; Saleem, M.; Mallick, B. C.; Jha, S. The effects of 992 interfacial potential on antimicrobial propensity of ZnO nanoparticle. *993 Sci. Rep.* **2015**, *5*, No. 9578.

994 (41) Fatimah, I.; Pradita, R. Y.; Nurhalinda, A. Plant extract mediated 995 of ZnO nanoparticles by using ethanol extract of *Mimosa pudica* leaves 996 and coffee powder. *Procedia Eng.* **2016**, *148*, 43–48.

997 (42) Rajiv, P.; Rajeshwari, S.; Venkatesh, R. Bio-Fabrication of zinc 998 oxide nanoparticles using leaf extract of *Parthenium hysterophorus* L.

1000 and its size-dependent antifungal activity against plant fungal
1001 pathogens. *Spectrochim. Acta, Part A* **2013**, *112*, 384–387.

1002 (43) Pillai, A. M.; Sivasankarapillai, V. S.; Rahdar, A.; Joseph, J.;
1003 Sadeghfar, F.; Rajesh, K.; Kyzas, G. Z.; et al. Green synthesis and
1004 characterization of zinc oxide nanoparticles with antibacterial and
1005 antifungal activity. *J. Mol. Struct.* **2020**, *1211*, No. 128107.

1006 (44) Modena, M. M.; Röhle, B.; Burg, T. P.; Wuttke, S. Nanoparticle
1007 Characterization: Nanoparticle Characterization: What to Measure?
1008 *Adv. Mater.* **2019**, *31*, No. 1970226.

1009 (45) Vimala, K.; Sundarraj, S.; Paulpandi, M.; Vengatesan, S.;
1010 Kannan, S. Green synthesized doxorubicin loaded zinc oxide
1011 nanoparticles regulates the Bax and Bcl-2 expression in breast and
1012 colon carcinoma. *Process Biochem.* **2014**, *49*, 160–172.

1013 (46) Lynch, I.; Dawson, K. A. Protein-nanoparticle interactions.
1014 *Nano Today* **2008**, *3*, 40–47.

1015 (47) Romero, C. D.; Chopin, S. F.; Buck, G.; Martinez, E.; Garcia,
1016 M.; Bixby, L. Antibacterial properties of common herbal remedies of
1017 the southwest. *J. Ethnopharmacol.* **2005**, *99*, 253–257.

1018 (48) Boucher, H. W.; Talbot, G. H.; Bradley, J. S.; Edwards, J. E.;
1019 Gilbert, D.; Rice, L. B.; Scheld, M.; Spellberg, B.; Bartlett, J. Bad bugs,
1020 no drugs: no ESKAPE! An update from the Infectious Diseases
1021 Society of America. *Clin. Infect. Dis.* **2009**, *48*, 1–12.

1022 (49) Talbot, G. H.; Bradley, J.; Edwards, J. E., Jr.; Gilbert, D.;
1023 Scheld, M.; Bartlett, J. G. Bad bugs need drugs: an update on the
1024 development pipeline from the Antimicrobial Availability Task Force
1025 of the Infectious Diseases Society of America. *Clin. Infect. Dis.* **2006**,
1026 *42*, 657–668.

1027 (50) Rajeshkumar, S.; Menon, S.; Kumar, S. V.; Tambuwala, M. M.;
1028 Bakshi, H. A.; Mehta, M.; Satija, S.; Gupta, G.; Chellappan, D. K.;
1029 Thangavelu, L. Antibacterial and antioxidant potential of biosynthe-
1030 sized copper nanoparticles mediated through *Cissus arnotiana* plant
1031 extract. *J. Photochem. Photobiol. B* **2019**, *197*, No. 111531.

1032 (51) Faisal, S.; Khan, M. A.; Jan, H.; Shah, S. A.; Shah, S.; Rizwan,
1033 M.; Ullah, W.; Akbar, M. T. Edible mushroom (*Flammulina velutipes*)
1034 as biosource for silver nanoparticles: from synthesis to diverse
1035 biomedical and environmental applications. *Nanotechnology* **2020**, *32*,
1036 No. 065101.

1037 (52) Awwad, A. M.; Amer, M. W.; Salem, N. M.; Abdeen, A. O.
1038 Green synthesis of zinc oxide nanoparticles (ZnO-NPs) using
1039 *Ailanthus altissima* fruit extracts and antibacterial activity. *Chem. Int.*
1040 **2020**, *6*, 151–159.

1041 (53) Roux, P. P.; Blenis, J. ERK and p38 MAPK-activated protein
1042 kinases: a family of protein kinases with diverse biological functions.
1043 *Microbiol. Mol. Biol. Rev.* **2004**, *68*, 320–344.

1044 (54) Pathania, D.; Millard, M.; Neamati, N. Opportunities in
1045 discovery and delivery of anticancer drugs targeting mitochondria and
1046 cancer cell metabolism. *Adv. Drug Delivery Rev.* **2009**, *61*, 1250–1275.

1047 (55) Mohamed, H. E. A.; Afridi, S.; Khalil, A. T.; Zia, D.; Shinwari,
1048 Z. K.; Dhlamini, M. S.; Maaza, M. Structural, morphological and
1049 biological features of ZnO nanoparticles using *Hyphaene thebaica* (L.)
1050 Mart. fruits. *J. Inorg. Organomet. Polym. Mater.* **2020**, *30*, 3241–3254.

1051 (56) Nair, A.; Jayakumari, C.; Jabbar, P.; Jayakumar, R.; Raizada, N.;
1052 Gopi, A.; George, G. S.; Seena, T. Prevalence and associations of
1053 hypothyroidism in Indian patients with type 2 diabetes mellitus. *J.*
1054 *Thyroid Res.* **2018**, *2018*, No. 5386129.

1055 (57) Aynalem, S. B.; Zeleke, A. J. Prevalence of diabetes mellitus and
1056 its risk factors among individuals aged 15 years and above in Mizan-
1057 Aman town, Southwest Ethiopia, 2016: a cross sectional study. *Int. J.*
1058 *Endocrinol.* **2018**, *2018*, No. 9317987.

1059 (58) Thiruvengadam, M.; Chung, I.-M.; Gomathi, T.; Ansari, M. A.;
1060 Khanna, V. G.; Babu, V.; Rajakumar, G. Synthesis, characterization
1061 and pharmacological potential of green synthesized copper nano-
1062 particles. *Bioprocess Biosyst. Eng.* **2019**, *42*, 1769–1777.

1063 (59) Vasudeo, K.; Pramod, K. Biosynthesis of nickel nanoparticles
1064 using leaf extract of coriander. *Biotechnology* **2016**, *12*, 1–6.

1065 (60) Sergiev, I.; Todorova, D.; Shopova, E.; Jankauskiene, J.;
1066 Jankovska-Bortkevič, E.; Jurkonienė, S. Exogenous auxin type
1067 compounds amend PEG-induced physiological responses of pea
1068 plants. *Sci. Hortic.* **2019**, *248*, 200–205.

1069 (61) Mohamed, H. I.; Akladious, S. A. Changes in antioxidants 1070
1071 potential, secondary metabolites and plant hormones induced by 1070
1072 different fungicides treatment in cotton plants. *Pestic. Biochem. Physiol.* 1071
1073 **2017**, *142*, 117–122.

1074 (62) Rehman, M.; Ullah, S.; Bao, Y.; Wang, B.; Peng, D.; Liu, L. 1073
1075 Light-emitting diodes: whether an efficient source of light for indoor 1074
1076 plants? *Environ. Sci. Pollut. Res.* **2017**, *24*, 24743–24752.

1077 (63) Prieto, M.; Curran, T. P.; Gowen, A.; Vázquez, J. A. An efficient 1076
1078 methodology for quantification of synergy and antagonism in single 1077
1079 electron transfer antioxidant assays. *Food Res. Int.* **2015**, *67*, 284–298.

1080 (64) Stanislavljević, N.; Bajić, S. S.; Jovanović, Ž.; Matić, I.; 1080
1081 Tolinački, M.; Popović, D.; Popović, N.; Terzić-Vidojević, A.; Golić, 1080
1082 N.; Beškoski, V.; et al. Antioxidant and antiproliferative activity of 1081
1083 *Allium ursinum* and their associated microbiota during simulated 1082
1084 in vitro digestion in the presence of food matrix. *Front. Microbiol.* **2020**, 1083
1085 *11*, No. 601616.

1086 (65) Skonieczna, M.; Hudy, D. Biological Activity of Silver 1085
1087 Nanoparticles and Their Applications in Anticancer Therapy. In 1086
1088 *Silver Nanoparticles: Fabrication, Characterization and Applications*; 1087
1089 2018; p 131.

1090 (66) Ul-Haq, I.; Ullah, N.; Bibi, G.; Kanwal, S.; Ahmad, M. S.; 1089
1091 Mirza, B. Antioxidant and cytotoxic activities and phytochemical 1090
1092 analysis of *Euphorbia wallichii* root extract and its fractions. *Iran. J. 1091*
1093 *Pharm. Res.* **2012**, *11*, 241.

1094 (67) Khalil, A. T.; Ovais, M.; Ullah, I.; Ali, M.; Shinwari, Z. K.; 1093
1095 Hassan, D.; Maaza, M. *Sageretia thea* (Osbeck.) modulated biosyn- 1094
1096 thesis of NiO nanoparticles and their in vitro pharmacognostic, 1095
1097 antioxidant and cytotoxic potential. *Artif. Cells, Nanomed., Biotechnol.* 1096
1098 **2018**, *46*, 838–852.

1099 (68) Akbari, M.; Oryan, A.; Hatam, G. Application of nano- 1098
1100 technology in treatment of leishmaniasis: A Review. *Acta Trop.* **2017**, 1099
1101 *172*, 86–90.

1102 (69) Jebali, A.; Kazemi, B. Nano-based antileishmanial agents: a 1101
1103 toxicological study on nanoparticles for future treatment of cutaneous 1102
1104 leishmaniasis. *Toxicol. In Vitro* **2013**, *27*, 1896–1904.

1105 (70) Jan, H.; Khan, M. A.; Usman, H.; Shah, M.; Ansir, R.; Faisal, S.; 1104
1106 Ullah, N.; Rahman, L. The *Aquilegia pubiflora* (Himalayan columbine) 1105
1107 mediated synthesis of nanoceria for diverse biomedical applications. 1106
1108 *RSC Adv.* **2020**, *10*, 19219–19231.

1109 (71) World Health Organization. *Comprehensive Guideline for 1108
1110 Prevention and Control of Dengue and Dengue Haemorrhagic Fever*, 2011.

1111 (72) Johnson, N.; de Marco, M. F.; Giovannini, A.; Ippoliti, C.; 1111
1112 Danzetta, M. L.; Svartz, G.; Erster, O.; Groschup, M. H.; Ziegler, U.; 1112
1113 Mirazimi, A.; et al. Emerging mosquito-borne threats and the 1113
1114 response from European and eastern Mediterranean countries. *Int. 1114*
1115 *J. Environ. Res. Public Health* **2018**, *15*, No. 2775.

1116 (73) Brix, K. V.; Cardwell, R. D.; Adams, W. J. Chronic toxicity of 1116
1117 arsenic to the Great Salt Lake brine shrimp, *Artemia franciscana*. 1117
1118 *Ecotoxicol. Environ. Saf.* **2003**, *54*, 169–175.

1119 (74) Ozkan, Y.; Altinok, I.; İlhan, H.; Sokmen, M. Determination of 1119
1120 TiO₂ and AgTiO₂ nanoparticles in *Artemia salina*: toxicity, 1120
1121 morphological changes, uptake and depuration. *Bull. Environ. Contam. 1121*
1122 *Toxicol.* **2016**, *96*, 36–42.

1123 (75) Klaine, S. J.; Alvarez, P. J.; Batley, G. E.; Fernandes, T. F.; 1123
1124 Handy, R. D.; Lyon, D. Y.; Mahendra, S.; McLaughlin, M. J.; Lead, J. 1124
1125 R. Nanomaterials in the environment: behavior, fate, bioavailability, 1125
1126 and effects. *Environ. Toxicol. Chem.* **2008**, *27*, 1825–1851.

1127 (76) Khoshnood, R.; Jaafarzadeh, N.; Jamili, S.; Farshchi, P.; 1127
1128 Taghavi, L. Acute toxicity of TiO₂, CuO and ZnO nanoparticles in 1128
1129 brine shrimp, *Artemia franciscana*. *Iran. J. Fish. Sci.* **2017**, *16*, 1287– 1129
1130 1296.

1131 (77) Nasar, M. Q.; Khalil, A. T.; Ali, M.; Shah, M.; Ayaz, M.; 1131
1132 Shinwari, Z. K. Phytochemical analysis, *Ephedra Procera CA Mey.* 1132
1133 Mediated green synthesis of silver nanoparticles, their cytotoxic and 1133
1134 antimicrobial potentials. *Medicina* **2019**, *55*, No. 369.

1135 (78) Sajadi, S. M.; Kolo, K.; Hamad, S. M.; Mahmud, S. A.; Barzinjy, 1135
1136 A. A.; Hussein, S. M. Green Synthesis of the Ag/Bentonite 1136
1137 Nanocomposite Using *Euphorbia larica* Extract: A Reusable Catalyst 1137

1138 for Efficient Reduction of Nitro Compounds and Organic Dyes.
1139 *ChemistrySelect* **2018**, *3*, 12274–12280.

1140 (79) Su, Y.; Yang, Y.; Zhang, H.; Xie, Y.; Wu, Z.; Jiang, Y.; Fukata, N.; Bando, Y.; Wang, Z. L. Enhanced photodegradation of methyl orange with TiO_2 nanoparticles using a triboelectric nanogenerator. *Nanotechnology* **2013**, *24*, No. 295401.

1141 (80) Holzwarth, U.; Gibson, N. The Scherrer equation versus the Debye–Scherrer equation. *Nat. Nanotechnol.* **2011**, *6*, 534.

1142 (81) Barzinjy, A.; Mustafa, S.; Ismael, H. Characterization of ZnO NPs prepared from green synthesis using *Euphorbia Petiolata* leaves. *Eurasian J. Sci. Eng.* **2019**, *4*, 74–83.

1143 (82) Morais, M.; Namouni, F. Asteroids in retrograde resonance with Jupiter and Saturn. *Mon. Not. R. Astron. Soc.: Lett.* **2013**, *436*, L30–L34.

1144 (83) Shah, M.; Nawaz, S.; Jan, H.; Uddin, N.; Ali, A.; Anjum, S.; Giglioli-Guivarc'h, N.; Hano, C.; Abbasi, B. H. Synthesis of bio-mediated silver nanoparticles from *Silybum marianum* and their biological and clinical activities. *Mater. Sci. Eng. C* **2020**, *112*, No. 110889.

1145 (84) Faisal, S.; Khan, M. A.; Jan, H.; Shah, S. A.; Abdullah, A.; Shah, S.; Rizwan, M.; Ullah, W.; Akbar, M. T.; Redaina, R. Edible Mushroom (*Flammulina velutipes*) as Biosource for Silver Nano-particles: From Synthesis to Diverse Biomedical and Environmental Applications *Nanotechnology* **2020** *32* 6 DOI: 10.1088/1361-6528/abc2eb.

1146 (85) Usman, H.; Ullah, M. A.; Jan, H.; Siddiquah, A.; Drouet, S.; Anjum, S.; Giglioli-Guivarc'h, N.; Hano, C.; Abbasi, B. H. Interactive Effects of wide-spectrum monochromatic lights on phytochemical production, antioxidant and biological activities of *Solanum xanthocarpum* callus cultures. *Molecules* **2020**, *25*, No. 2201.

1147 (86) Nazir, S.; Jan, H.; Tungmunnithum, D.; Drouet, S.; Zia, M.; Hano, C.; Abbasi, B. H. Callus Culture of Thai Basil Is an Effective Biological System for the Production of Antioxidants. *Molecules* **2020**, *25*, No. 4859.

1148 (87) Abdel-Aziz, H. M.; Rizwan, M. Chemically synthesized silver nanoparticles induced physio-chemical and chloroplast ultrastructural changes in broad bean seedlings. *Chemosphere* **2019**, *235*, 1066–1072.

1149 (88) Soflaei, S.; Dalimi, A.; Abdoli, A.; Kamali, M.; Nasiri, V.; Shakibaie, M.; Tat, M. Anti-leishmanial activities of selenium nanoparticles and selenium dioxide on *Leishmania infantum*. *Comp. Clin. Pathol.* **2014**, *23*, 15–20.

1150 (89) Gerberg, E. J.; Barnard, D. R.; Ward, R. A. *Manual for Mosquito Rearing and Experimental Techniques*; American Mosquito Control Association, Inc., 1994.

1151 (90) Elango, G.; Roopan, S. M.; Al-Dhabi, N. A.; Arasu, M. V.; Dhamodaran, K. I.; Elumalai, K. Coir mediated instant synthesis of Ni-Pd nanoparticles and its significance over larvicidal, pesticidal and ovicidal activities. *J. Mol. Liq.* **2016**, *223*, 1249–1255.

1152 (91) Kumar, K. P.; Paul, W.; Sharma, C. P. Green synthesis of gold nanoparticles with *Zingiber officinale* extract: characterization and blood compatibility. *Process Biochem.* **2011**, *46*, 2007–2013.

1153 (92) Nasrollahzadeh, M.; Sajjadi, M.; Maham, M.; Sajadi, S. M.; Barzinjy, A. A. Biosynthesis of the palladium/sodium borosilicate nanocomposite using *Euphorbia milii* extract and evaluation of its catalytic activity in the reduction of chromium (VI), nitro compounds and organic dyes. *Mater. Res. Bull.* **2018**, *102*, 24–35.